Clays and Clay Minerals, Vol. 47, No. 5, 582–590, 1999.

CRYSTAL CHEMISTRY OF LAYER SILICATES OF THE MIOCENE GREEN GRAIN (CONGO BASIN) FROM TRANSMISSION ELECTRON MICROSCOPY (TEM) AND ANALYTICAL ELECTRON MICROSCOPY (AEM) OBSERVATIONS

A. WIEWIÓRA,[1] P. GIRESSE,[2] A. M. JAUNET,[2] A. WILAMOWSKI,[1] AND F. ELSASS[3]

[1] Institute of Geological Sciences, Polish Academy of Sciences, ul. Twarda 51/55, 00-818, Warszawa, Poland
[2] Laboratoire de Sédimentologie et Géochimie marine, URA CNRS 715, LEA Sciences de la Mer, Université de Perpignan, Avenue de Villeneuve, 66860 Perpignan, France
[3] Sciences du Sol, INRA, Route de Saint Cyr, 78026 Versailles, France

Abstract—Transmission electron microscopy (TEM) and analytical electron microscopy (AEM) methods were used to study the crystal chemistry of phyllosilicates occurring in green grains of Miocene sediments from the Congo continental shelf. Using diagrams based on wt. % K and the (Fe + Mg)/Al ratio, minerals were distinguished from mixed-layer phases. The most abundant detrital mineral is Fe-kaolinite. The morphology and composition identify this mineral as a component of ferralitic soils. This Fe-rich kaolinite has undergone a complex process of partial dissolution and recrystallization and further enrichment in Fe and, to a lesser extent, in Mg in the marine environment. The detrital mica observed with TEM retains the original morphology and chemistry of muscovite. Alteration processes resulted in the crystallization of 1:1 trioctahedral Fe^{2+} and Mg-rich minerals and interstratified phases with 1:1 and 2:1 layers in varying proportions observed with the aid of high-resolution transmission electron microscopy (HRTEM) imaging. Included among the newly formed 7-Å phases are those apparently containing excess Si. The smectites are apparently neoform, and chemical analyses showed that these marine K-smectites belong to the beidellite-nontronite series and have tetrahedral substitutions similar to muscovite. Their compositions are closer to beidellite than to nontronite, although the latter was observed in association with goethite. The TEM observations and crystallochemical data show that mineral alteration ceased after forming mixed-layer minerals, and alteration did not reach the glauconitization stage. Apparently, the Miocene assemblages experienced rapidly changing environmental conditions and high sedimentation rates that continue today.

Key Words—Alteration Markers, Congo Basin, Detrital Phyllosilicates, Green Grains, Neoformed Phyllosilicates.

INTRODUCTION

Fecal pellets from the continental shelves of tropical latitudes are characterized by restricted interactions with their local seawater environments. Exchanges between seawater and pellets involve primarily Fe in the sediments (Giresse, 1985). In these pellets, various evolutionary processes (alteration and neoformation) occur and the products add to various inherited detrital phases (kaolinite, quartz, amorphous iron hydroxides, goethite, and occasionally large muscovite flakes). Analysis of grain populations from the Gulf of Guinea by X-ray diffraction (XRD) revealed the presence of a dominant 7-Å Fe-rich phase which was identified variously as chamosite (Von Gaertner and Schellman, 1965; Porrenga, 1967), as poorly crystallized berthierine (Giresse and Odin, 1973), and finally as odinite (phyllite V) from the verdine facies (Bailey, 1988; Odin *et al.*, 1988).

High-resolution transmission electron microscopy (HRTEM) was previously used to study the structure and growth mechanism of Paleocene glauconite of the Côte d'Ivoire (Amouric and Parron, 1985). Formation of this glauconite appears to have involved crystallization, dissolution, mass transfer, and neocrystallization within a gel rather than direct solid-state transformation from a pre-existing mineral. In another study (Odin *et al.*, 1988), various green grains belonging to the verdine facies were collected from Recent sediments of the shelves of New Caledonia, Guinea, and Senegal. HRTEM analysis identified two types of verdine in these grains, the first mostly composed of 7-Å thick layers is known to be Recent in age, and the second contains mixtures of 7-, 10-, and 14-Å microcrystals and comprises the more ancient verdines.

Samples from Recent sediments off the mouth of the Congo River were studied by the separation of the green peloids into different density fractions. These fractions contained either mostly phyllosilicates or goethite, thereby enabling the study of the crystal chemistry of the individual phases with some precision (Giresse *et al.*, 1988). The 10-Å minerals in grains deposited in the sediment of the outer shelf have a homogeneous composition and occur in association with goethite and quartz. The green Fe-bearing peloids containing 7-Å Fe-rich phases were deposited in an area with a high sedimentation rate off the Congo River. The chemical composition suggested the transfor-

mation of kaolinite into a 7-Å Fe-rich phase via substitution of Fe^{2+} and Mg for Al in the octahedral sheet, with minor changes in the tetrahedral sheet.

XRD analyses of mixtures of different grains from the Congolese basin were supplemented by diffraction analyses of the individual grains. XRD using a position-sensitive detector (PSD) was used simultaneously with energy-dispersive spectrometry (EDS), for structural and chemical characterization. In addition, scanning electron microscopy (SEM) was used to characterize the chemical components of fecal pellets from the Miocene period to Recent on the shelf close to the mouth of the Congo River (Wiewióra *et al.*, 1996). XRD studies of single grains, using a PSD, demonstrated the polymineralic character of the grains. The primary phyllosilicates include nontronite, kaolinite, Fe-containing 7-Å phases having larger *b* unit-cell parameters than kaolinite, and interstratified phases with 7- and 10-Å layers. The chemical composition changes from grain to grain. The precise structural formulae of the Fe-containing 7-Å phases could not be determined due to contamination by interstratified 10-Å phases.

Kaolinite is abundant in the Recent peloids, whereas the dioctahedral Fe^{3+}-bearing 1:1 phases (Fe-kaolinite) are more abundant within the more mature Miocene peloids (Wiewióra *et al.*, 1996). The latter are also characterized by abundant K-bearing nontronite formed via neoformation rather than alteration of preexisting phases. However, these processes do not suggest a burial influence. The Holocene section suggests that these processes are related to accumulation rate; on this time scale the duration of mineral-sea water interaction (early diagenesis) is more important than burial (late diagenesis).

A study of a 7-Å Fe-rich phase and its transformation in Recent fecal pellets of the Congolese shelf was conducted using HRTEM combined with microchemical EDS analyses (Amouric *et al.*, 1995). This study emphasized the polymineralic nature (mainly 1:1 and 2:1 phyllosilicate phases) of the pellets. From an original Fe-rich kaolinite, successive dissolution-recrystallization reactions took place to form a new 7-Å Fe-rich phase, the composition of which varies from an intermediate dioctahedral-trioctahedral mineral to a trioctahedral (Mg + Fe) mineral. The crystallization of dioctahedral K-rich mica-like layer silicates may occur at the expense of this 7-Å Fe-rich phase and/or via dissolution-recrystallization. This reaction series progresses through interstratified structures with 1:1 and 2:1 layers. According to Amouric *et al.* (1995), these trends may represent the beginning of the glauconitization process.

In the present work, considering the polymineralic nature of the grains, TEM was used to supplement previous results (Wiewióra *et al.*, 1996). Earlier results suffered from the use of analytical methods that involved microscopic studies, coupled with the very small size of all phases present, especially those recrystallized or neoformed. A complete mineralogical and geochemical description of these green grains must consider the entire evolutionary process. We selected Miocene grains of the Congo continental shelf from petroleum drill cores at a depth of 230 m. These grains show evolutionary changes similar to those occurring with Recent grains, although most of these grains have greater quantities of reaction products than Recent material. The application of TEM permitted us to study the morphology and chemistry of the coarse- and the fine-scale mineral phases and to identify the interstratified phases. These data established crystallochemical markers, which provided information on the recrystallization processes.

SEDIMENTOLOGICAL SETTING

A humid tropical climate has prevailed since the beginning of the Miocene in the Congo Basin (Maley, 1996; Siesser, 1978). The proportion of coarse-grained deposits increased during the Neogene, especially adjacent to major rivers, *e.g.*, the Congo River where increased amounts of kaolinite (>50%) are observed in the clay assemblage. This area also contains higher concentrations of Fe^{3+} in the marine muds (>10%) and more green grains, mostly fecal pellets (Oualembo-Mophawe, 1992). Such green grains contain 1:1 and 2:1 layer silicates and, in some cases, constitute nearly 15% of the sand fraction. Based on the palynological study of Neogene sediments of the area (Poumot, 1989), there is evidence for nearly constant conditions favorable for glauconitization until Recent time. The beginning of this favorable environment coincides with the development of a general progradational depositional succession, succeeded from previous aggradational formations (Séranne *et al.*, 1992).

As noted above, similar glauconitization processes were observed in marine green grains belonging to the Miocene and the Recent of the Congo Basin. However, the Miocene deposits are inferred to represent a variable sedimentation rate because of their thickness, to 700 m in the studied bore-hole. We have selected gray-green peloids without fissures and with the same morphology as those previously described as representative of a mid-evolutionary state process (Wiewióra *et al.*, 1996).

METHODS

Samples for TEM observation were dehydrated using successive baths of methanol and propylene oxide (Elsass *et al.*, 1998) and then embedded in Spurr resin. After polymerization of the resin at 60°C, 50-nm thick sections were cut by ultramicrotomy using a Reichert Ultracut E microtome. A Philips 420 STEM electron microscope at 120 kV accelerating voltage with a 40 μm objective aperture was used. The conditions were similar to those used by Środoń *et al.* (1990). TEM

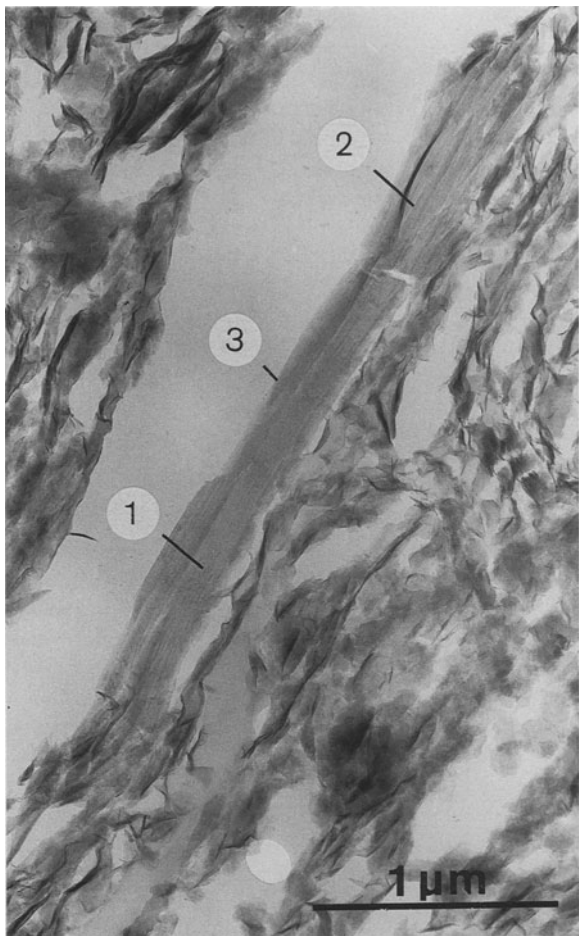

Figure 1. TEM micrograph of a muscovite flake along a fissure (microtome artifact). The spots refer to points where chemical analyses were taken (Table 1).

images were recorded only from areas of the specimens showing good contrast and morphological detail. Each image was complemented by EDS analyses. Measurements from images were made from the negative by using a stereo-microscope equipped with a micrometer scale. Values of interlayer spacings were obtained by dividing the thickness of the stack of layers of identical spacings by the number of interlayers. Thickness was measured between the centers of the two external layers, at the maximum intensity of the lattice fringe. EDS analyses were made with a Link system (AN 10,000) with a beam size of 40–200 nm, depending on the size of an analyzed object. The data were interpreted with caution because of possible affects of radiation damage during exposure. The relative error in X-ray analysis by analytical electron microscopy (AEM) is often >5% (Warren and Ransom, 1992).

RESULTS

Forty-one chemical analyses were made on the studied material portrayed on 19 photographs. Enlargements were made of selected regions of the crystals that were both imaged and chemically analyzed for visualization of layer sequences and mixed layering. TEM images with their associated AEM analyses allowed us to distinguish distinct phyllosilicates differing in shape, size, and chemical composition. Mica, Fe-rich kaolinite, neoformed smectite, kaolinite, and mixed-layer phases comprising various proportions of 7- and 10-Å phyllosilicates were recognized based on TEM and AEM observations. Multiple observations minimized ambiguity in classifying grains.

EDS analyses can not provide a determination of iron oxidation state. Therefore, the composition expressed by the crystallochemical formula was presented in two versions, either with total iron as Fe^{3+} or as Fe^{2+}. This approach was used for presentation of the crystal chemistry of muscovite, smectite, and Fe-kaolinite. For other phases, we made no assumptions on the iron oxidation state or type of layer (2:1, 1:1, or mixture of the two). In such cases, chemical data are presented diagrammatically using the raw elemental compositions expressed in weight percent.

Figure 1 shows a thin (0.2 µm) and very elongated (4 µm) flake composed of packets ~0.1 µm in length. The flake stretches at the margin of the clay matrix along the fissure (microtome artifact) and is well distinguished from the surrounding finer flakes in the matrix. The most distinct feature of this flake is its homogeneity and sharp boundaries between domains. The habit and composition determined at three points on the flake (points 1, 2, 3 in Table 1), and the high K content (close to 1 per half formula unit, $O_{10}(OH)_2$, insert in Figure 2), indicate that it is a mica. The octahedral occupancy is between 2–2.12, with Al as the predominant octahedral cation (Figure 2), indicating a dioctahedral sheet (Table 2). Figure 3 presents the project field for K-micas (Wiewióra, 1990a) and shows that tetrahedral substitution is near $AlSi_3$, typical of muscovite. Thus, Figure 1 shows detrital muscovite that survived intact in the marine environment.

A different morphology from that common for muscovite is illustrated in Figure 4. Figure 4a shows a platy particle viewed along c^*, displaying hexagonal outlines. The particle appears compact with thick, homogenous packets ~0.08 µm in width. A similar packet thickness is observed in Figure 4b where a large flake that is cut quasi-perpendicular to the (001) plane is shown. Fragmentation of a large grain to smaller packets is observed in Figure 4a. Chemical data are designated by numbers in the figures. All show kaolinite composition. Only in point 8 (Figure 4a) was a measurable amount of K present (0.2 cation per half formula unit), which may indicate the initiation of formation of K-containing 2:1 layers or, alternately, the presence of residual K-mica.

Morphological forms typical of neoformed phases is shown in Figure 5. Very small grains (~0.1 µm)

https://doi.org/10.1346/CCMN.1999.0470505 Published online by Cambridge University Press

Table 1. Point chemical compositions (in wt. %) adjusted to 100%.

Point	SiO_2	TiO_2	Al_2O_3	Fe_2O_3	MgO	K_2O
1	47.90	0.04	38.38	1.44	0.00	12.24
2	46.68	0.15	38.41	2.00	1.41	11.36
3	46.83	0.17	39.77	1.53	0.45	11.25
4	48.07	0.67	30.07	8.72	4.56	7.90
5	50.24	0.04	32.42	6.91	3.49	6.90
6	50.37	0.09	32.51	6.65	4.27	6.12
7	54.34	0.09	29.39	6.12	4.95	5.11
8	47.28	0.00	25.83	16.87	5.91	4.11
9	47.97	0.52	38.39	10.49	2.48	0.15
10	50.13	0.00	37.50	10.62	1.46	0.29
11	46.98	0.00	30.12	14.48	6.10	2.31
12	49.49	0.05	33.11	12.24	4.59	0.53
13	52.56	0.11	25.01	15.63	0.00	6.68
14	54.08	4.45	24.97	13.26	3.24	0.00
15	66.38	0.00	20.64	12.89	0.00	0.09
16	48.86	0.84	16.01	23.41	8.87	2.01
17	49.33	0.97	18.73	23.32	6.25	1.41
18	47.91	0.50	22.32	18.99	5.61	4.66
19	48.72	0.33	10.17	26.55	9.93	4.30
20	46.03	2.71	9.72	30.85	9.05	1.64
21	48.26	0.11	15.59	19.81	8.55	7.68
22	48.26	0.11	15.59	19.81	8.55	7.68
23	46.98	0.02	17.07	26.44	6.70	2.79
24	46.23	0.02	16.36	25.02	9.43	2.94
25	47.92	0.19	20.66	21.71	6.83	2.68
26	50.19	0.19	16.19	24.75	6.96	1.72
27	47.65	0.56	13.19	31.66	6.44	0.51
28	41.29	1.20	15.25	31.86	9.12	1.28
29	47.51	0.39	31.14	7.74	3.50	9.72
30	51.03	0.00	16.59	21.04	8.03	3.31
31	48.84	0.00	17.06	22.66	9.89	1.54
32	49.67	0.00	18.93	21.55	8.49	1.36
33	47.62	0.00	14.95	23.80	9.92	3.70
34	48.94	0.21	17.76	20.48	8.82	3.79
35	48.42	0.02	17.77	21.98	9.85	1.96
36	51.53	0.48	24.24	16.40	4.93	2.42
37	47.60	0.00	22.27	17.07	8.73	4.33
38	47.84	0.00	17.35	24.35	9.63	0.82
39	50.16	0.02	13.35	25.00	9.69	1.78
40	47.54	0.00	15.56	24.60	10.60	1.70
41	49.75	0.07	14.02	25.87	8.29	2.00

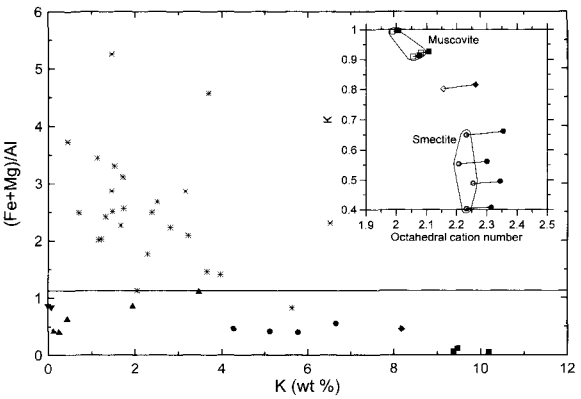

Figure 2. Relationship between K-content and (Fe + Mg/Al) for all studied compositions: squares micas, circles: smectites, triangles: Fe-kaolinites, stars: mixed phases, diamond: high K mixed phase. The relationship between K and octahedral-cation content in 2:1 phases is presented in the inset in which the oxidation state of iron is differentiated. Empty pictogram: analyses with Fe^{3+}, filled: analyses with Fe^{2+}.

are distributed near the void. These flakes are identified as the "caterpillar-like" edges on the rims of the larger flakes of smectite observed by SEM (Wiewióra *et al.*, 1996). The compositions determined on seven different flakes (points 4, 5, 6; Figure 5) are similar (Tables 1 and 2).

Potassium-free nanostructures are observed in Figure 4a near the Fe-rich kaolinite grain. The image shows well-shaped hexagonal crystallites and grains with frayed or destroyed edges. The latter probably crystallized by dissolution of kaolinite and subsequent crystallization. Chemical analysis (*e.g.*, point 14) of these flakes recalculated on the basis of $O_{10}(OH)_8$ shows excess Si and/or a large deficiency in octahedral cations. This composition does not plot on the projection plane of Figure 3, but plots above the plane, close to Si = 5 (inset in Figure 3). Because the upper limit is 4 for phyllosilicates, this analysis clearly represents contamination by colloidal silica or a high defect structure characterized by an increase in Si owing to a deficiency in octahedral cations. Similar chemistry is characteristic of point 15 and on other photographs (not shown).

K-containing phases are illustrated in Figure 6. The morphology is typical of phyllosilicates but they appear to be heterogeneous, based on 30 point analyses.

Table 2. Structural formulae of phases calculated per $O_{10}(OH)_2$ for mica and smectite and per $O_{10}(OH)_8$ for Fe-rich kaolinite.

	Muscovite			Smectite				Fe-rich kaolinite				
Point	1	2	3	4[1]	5	6	7	8	9	10	11	12
Si	3.04	2.97	2.97	3.09	3.15	3.15	3.35	3.94	3.75	3.88	3.81	3.89
^{IV}Al	0.96	1.03	1.03	0.91	0.85	0.85	0.65	0.06	0.25	0.12	0.19	0.11
^{VI}Al	1.92	1.85	1.94	1.37	1.55	1.54	1.49	2.48	3.28	3.30	2.69	2.96
Fe^{3+}	0.07	0.10	0.07	0.42	0.33	0.31	0.28	1.06	0.62	0.62	0.88	0.72
Mg	0.00	0.13	0.04	0.44	0.33	0.40	0.46	0.73	0.29	0.17	0.74	0.54
Σoct.	1.99	2.08	2.05	2.23	2.21	2.25	2.23	4.27	4.18	4.10	4.31	4.22
K	0.99	0.92	0.91	0.65	0.55	0.49	0.40					

[1] Five smectite individuals (Figure 5) showing the same composition.

https://doi.org/10.1346/CCMN.1999.0470505 Published online by Cambridge University Press

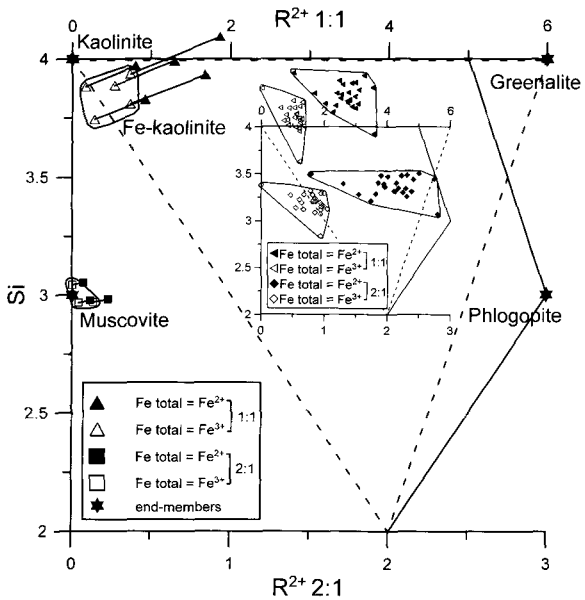

Figure 3. Relationship between Si (cations per four tetrahedral sites) and ΣR^{2+} (octahedral site) for the formula unit, $O_{10}(OH)_2$ (assuming 2:1 phyllosilicates) = lower scale, and for $O_{10}(OH)_8$ (assuming 1:1 phyllosilicates) = upper scale. Modified from Wiewióra (1990a, 1990b). Insert represents nonstoichiometric compositions. Note that the compositions, based on $O_{10}(OH)_8$ (1:1 phyllosilicates), fall outside of the projection field.

Packets are very thin (<0.01 μm) and folded. They are randomly distributed in the matrix. The K-content is below the detection limits in regions, whereas it ranges between 0–0.4 K per $O_{10}(OH)_2$ elsewhere, less than observed for smectites. Calculation on the basis of 14 oxygens (inset in Figure 3) also gave an anomalous result, giving a Si content >4. The observed composition thus suggests a mixed-layer phase.

HRTEM showed that most of these particles are composed mostly of 7-Å layers, although some outer layers are 10-Å layers. Enlargement of the flakes in Figure 6 revealed an interstratified structure where 7-Å layers dominate over 10-Å layers (Figure 7). These direct observations of 7-Å layers and mixed-layer grains of 7–10 Å confirm the earlier X-ray identification of a discrete trioctahedral 7-Å phase and of a randomly interstratified phase composed of trioctahedral 1:1 and dioctahedral 2:1 layers in an 85:15 proportion, as shown by simulation (Wiewióra *et al.*, 1996). In rare cases, spacings of 12 and 13 Å were identified. They apparently represent an uncommon 2:1 phyllosilicate with an expanded interlayer resembling smectitic layers.

CRYSTALLOCHEMICAL MARKERS OF ALTERATION AND NEOFORMATION PROCESSES

The trends in interlayer and octahedral cations (Figures 2 and 3), as shown by the chemical data combined with particle morphology, allowed the identification of the phyllosilicate phases as detrital muscovite, Fe-rich kaolinite, and neoformed smectite. Using the diagram based on wt. % K and the (Fe + Mg)/Al ratio, minerals were distinguished from mixed-layer phases. The discrimination line is drawn at an (Fe + Mg)/Al value of 1.1 (Figure 2), and the K content (inset) distinguishes the phases also. Figure 3 shows the crystal-chemical classification for micas and kaolinite-serpentines.

The observed muscovite (Figure 3) composition is near the end-member in the projection field ($0.9 < K < 1$; $2 < {}^{VI}R < 3$; Figure 2). Assumptions regarding the oxidation state of Fe in muscovite do not shift the points significantly. Such a highly aluminous, Fe-free, Mg-poor composition is characteristic of detrital muscovite and cannot be confused with illite and/or glauconite.

The compositions of the K-smectites (Figure 5) are plotted onto the projection field (Figure 8), which differs from that of the micas (Wiewióra, 1990a) by translation of the origin of the oblique axes from orthogonal *x*, *y* point coordinates 3, 3 to 3, 3.5. This shift is related to the lower layer charge in smectites (here at 0.5) than in micas (at 1 per formula unit). General formulae of the more important trioctahedral and dioctahedral smectite end-members are given. The observed compositions project near the pole $\Sigma R_2{}^{3+}\Sigma R_{0.25}{}^{2+}\square_{0.75}\ Si_3Al_1$. Compositions of K-rich nontronite, determined in the Miocene grains by EDS and SEM and by XRD techniques (Wiewióra *et al.*, 1966), also project near the same pole. Nontronites described by Stucki (1988) project between the two possible poles for nontronites-beidellites, most close to $\Sigma R_2{}^{3+}\square_1 Si_{3.5}Al_{0.5}$. On Figure 5 several flakes are observed that are similar in appearance, but distinct in morphology and chemistry (points 24, 25, 26). They would be erroneously classified as smectites if only morphology is considered, but the chemistry is unique. Projected points for these analyses do not fall in the field of smectite, but they fall in the middle of the region formed by the ill-defined phases (Figure 3).

The neoformed smectite shows 0.4–0.65 K per formula unit and the compositions of the octahedra and tetrahedra are defined by narrow limits. However, since the Fe content in the smectite is higher than in the mica (Table 2), the separation between points representing formulae with Fe^{3+} and with Fe^{2+} (inset in Figure 2) is greater than for the micas. Assuming all iron is ferric, the average structural formula for the smectite is: $K_{0.563}[(Al_{1.490}Fe^{3+}{}_{0.351}Mg_{0.387})(Si_{3.132}Al_{0.868})]O_{10}(OH)_2{\cdot}nH_2O$. The composition of the smectite occurring in the more evolved grain in the same population of Miocene grains determined by Wiewióra *et al.* (1996) is: $(K, Na, Ca/2)_{0.49}[(Fe^{3+}{}_{1.85}Mg_{0.5})(Si_{2.91}Al_{0.98}Fe_{0.11})]O_{10}(OH)_2{\cdot}nH_2O$, showing an iron content typical of nontronite. The composition of the smectite studied in this work cor-

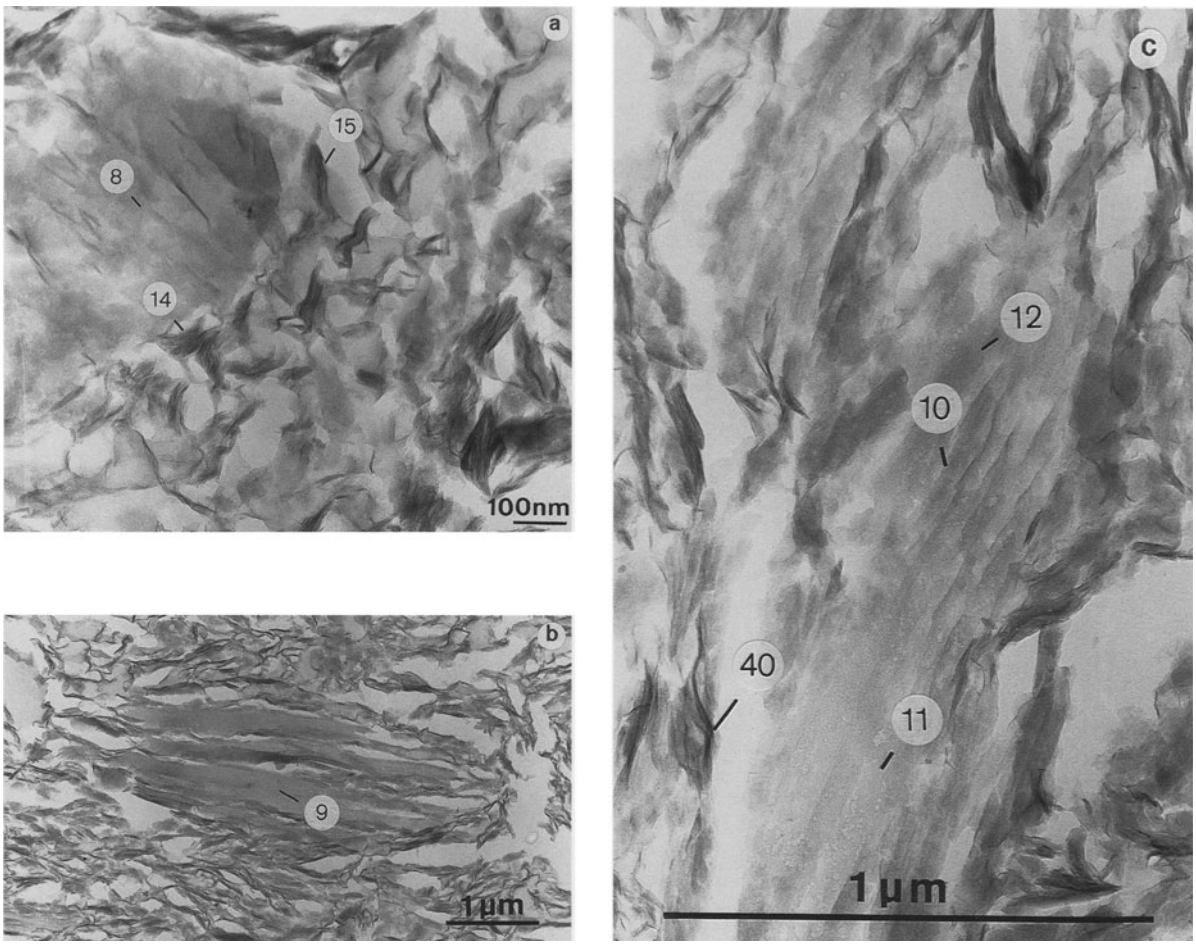

Figure 4. TEM micrographs of Fe-rich kaolinites: (a) isometric Fe-rich kaolinite plate displaying hexagonal subhedral edges. The plate is surrounded by minute neoformed wavy nanostructures; (b) Fe-rich kaolinite in the matrix of transformed material; (c) Fe-rich kaolinite with signs of alteration. Samples 8, 14, 15, 9, 10, 11, 12, 40 correspond with compositions shown in Table 1.

responds with Fe-rich beidellite rather than nontronite. K-rich beidellites and nontronites of marine origin (the present case) have higher substitutions in tetrahedral sites than the continental nontronites of Stucki (1988).

The Fe-rich kaolinites are K-free and are represented by the three compositions located near the origin of the orthogonal coordinate axis in Figure 2. The (Fe + Mg)/Al ratio is low (similar to smectites). If iron is ferric, then the projected points of all Fe-rich kaolinites are near the end-member composition of kaolinite (Figure 3). Most Fe-rich kaolinite flakes are Mg-free and differ from kaolinite only in Fe content. A relatively high iron content (0.6 to 1.0 cation per formula unit) may suggest that Fe-kaolinite originates from continental ferrallitic soils (Herbillon *et al.*, 1976; Mestdagh *et al.*, 1980; Nahon, 1981; Jepson, 1988; Stucki, 1988; Muller and Calas, 1993; Malengreau *et al.*, 1994).

Two point analyses showing some K content imply that the kaolinite grain, which exhibited a habit typical of detrital Fe-rich kaolinite, has undergone an initial stage of transformation to 2:1 layers. This process starts with an uptake of K (Figure 9a) which is evident by an increase of Fe and Mg content at the expense of Al (Figure 9b). Note that the two analyses of K-containing Fe-rich kaolinites may be incorporated equally well in the mixed-layer material in Figure 9b. However, those kaolinites have a habit more similar to the detrital Fe-rich kaolinite (Figure 4). The composition recalculated into structural formulae is projected to the field for the kaolinite-serpentine group. This is in contrast to mixed-layer material (Figure 7) where the chemical formulae based on $O_{10}(OH)_8$ fall outside the projected field (inset in Figure 2), thereby suggesting that they are not pure 7-Å minerals. HRTEM analyses clearly show the existence of randomly interstratified layers with different layer thickness typical for 1:1, 2:1, and possibly defect intermediate varieties. Thus, the structural formulae should not be determined on the basis of $O_{10}(OH)_8$ or $O_{10}(OH)_2$ as done

https://doi.org/10.1346/CCMN.1999.0470505 Published online by Cambridge University Press

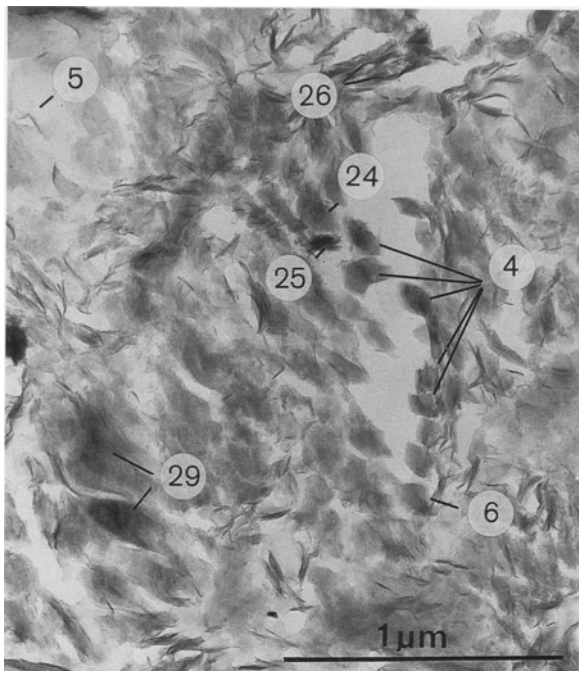

Figure 5. TEM micrograph of neoformed smectite nanostructures displayed around the void. Chemical compositions are in Table 1, under sample 4, 5, 6, 29. The surrounding material represents altered, mostly mixed-layer material, whose composition at the indicated points 24, 25, 26 is presented in Table 1.

by Amouric *et al.* (1995). The interstratified material cannot be distinguished easily from Fe-rich kaolinite using the diagram of Figure 9a, because both materials have low K-contents. Thus they project in the same field, but the position is distinct from that of the K-rich smectites and very K-rich muscovites. Differentiation is achieved by using a Si, Al, (Fe + Mg) triangular diagram (Figure 9b) where the chemical trend showing alteration is given. Figure 10, which shows more detail regarding the chemistry of the octahedral sheet, shows also that the process of transformation of Fe-containing primary kaolinite involves further enrichment in Fe at the expense of Al (Figure 10a) and

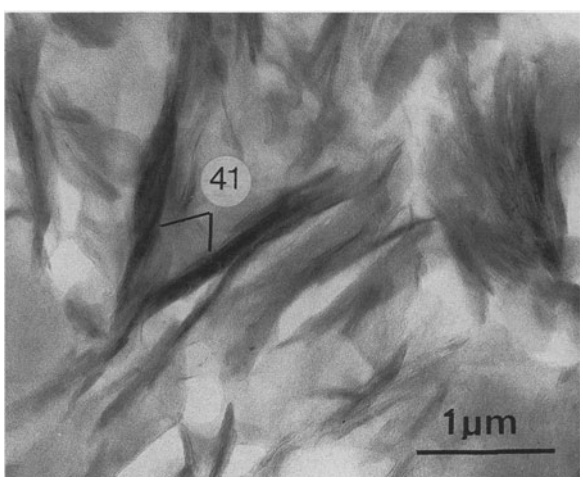

Figure 6. TEM micrographs of neoform phases; folded layer material forming V-shaped arrangement with visible packets. Sample composition 41 is in Table 1.

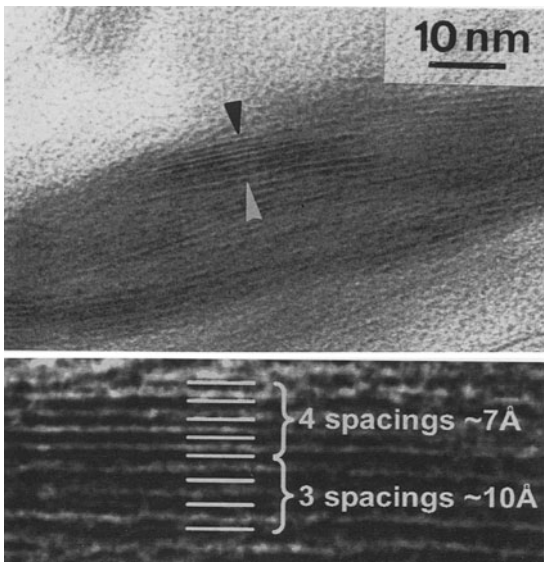

Figure 7. Lattice-fringe image observed on a layer stack from Figure 6. Computer-magnified interstratified stack composed of four 7-Å and three 10-Å layers is inset for better viewing.

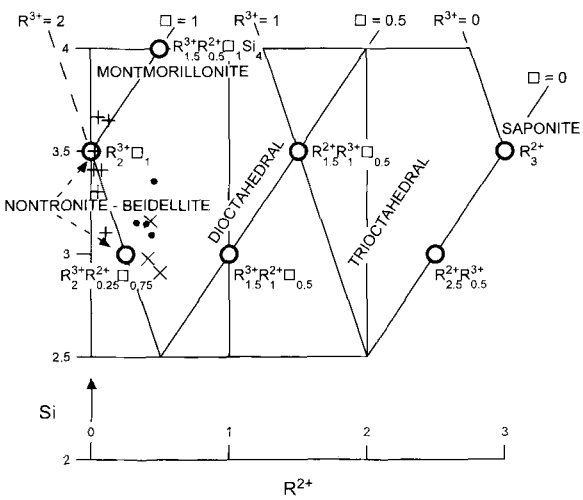

Figure 8. Projected field for composition of dioctahedral and trioctahedral smectites with a layer charge equal to 0.5 per formula unit. Structural formulae of Fe-rich beidellite (this work), and nontronites after Wiewióra *et al.* (1996) and Stucki (1988) are projected to the field. ×: Wiewióra *et al.* (1996); ●: AEM (this work); +: after Stucki (1988); ○: end-members.

https://doi.org/10.1346/CCMN.1999.0470505 Published online by Cambridge University Press

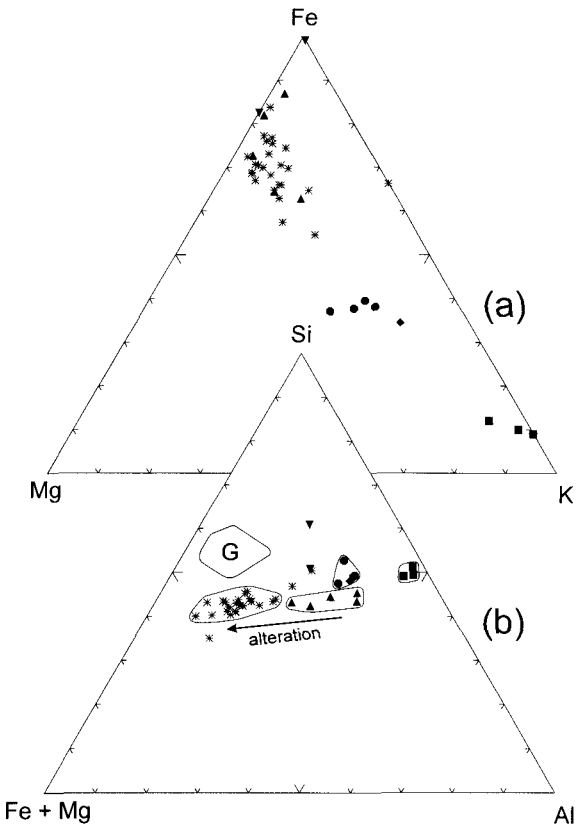

Figure 9. Triangular representation of the relationships between the major elements in the studied minerals within the Miocene green grains. Squares: micas, circles: smectites, triangles: Fe-rich kaolinites, inverted triangles: Fe-rich kaolinites with surplus Si, stars: mixed phases. In the diagram: (a) triangle K-Mg-Fe, (b) triangle Al-Fe + Mg-Si. G-composition field of glauconites from Recent grains, after Giresse *et al.* (1988).

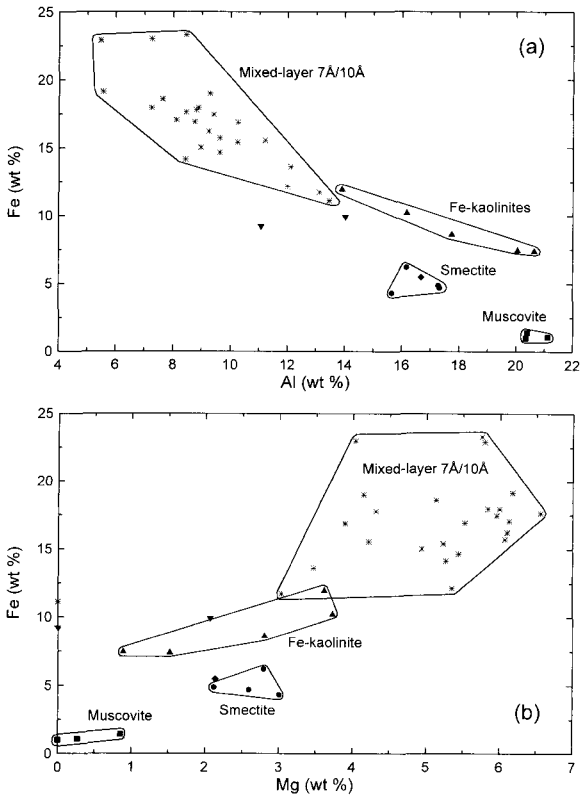

Figure 10. Relationship between (a) Fe vs. Al diagram and (b) Fe vs. Mg diagram. Symbols as in Figure 9. Notice distinct areas of projection points for all the studied minerals.

to a lesser extent Mg (Figure 10b). Also Mg content is related generally to an increase in Fe content.

CONCLUSIONS

The present study demonstrates that the phyllosilicate minerals present in the studied fecal pellets have a distinctive morphology and chemical composition. The mica in the pellets, present below the detection limits of powder XRD, has a morphology and composition typical of detrital muscovite. This detrital muscovite should not be confused with illite or glauconite.

The other relatively K-rich phase in the pellets is smectite. In the grains studied, this mineral has low Fe content and is classified as beidellite. Beidellite was not found by Wiewióra *et al.* (1996). In contrast to the detrital muscovite, smectite formed by direct crystallization from solution. The minute smectite flakes resemble nontronite flakes studied earlier by Wiewióra *et al.* (1996). There is not any apparent direct relationship between the smectite and muscovite. The difference in Fe content of the beidellite-type smectite (this work) and nontronite identified by Wiewióra *et al.* (1996) may result from competition for iron during mineral formation and the alteration processes.

Although solid-state transformation of smectite to glauconite is theoretically possible, especially considering their structural resemblance (Sakharov *et al.*, 1990), our TEM observations do not support such a process in the Miocene grains. Glauconite composition occurs far from the plotted composition of the studied smectites, and closer to the plotted composition of mixed-layer phases. We suggest that neoformation of glauconite occurs in off-shore quiescent zones during periods of low sedimentation rate.

Fe-rich kaolinites in Miocene grains were not previously identified unambiguously because of the multiphase and heterogeneous nature of the Miocene grains. The present study shows that the 7-Å phases are abundant in the Miocene grains, and their existence is not limited to Recent deposits.

The significant increase in Fe and, to a lesser extent in Mg, in the Fe-rich kaolinites during alteration involves recrystallization of the 7-Å layers into 10-Å layers. The last observed alteration product is the

https://doi.org/10.1346/CCMN.1999.0470505 Published online by Cambridge University Press

mixed-layer phase. As these Fe-rich phases are especially abundant in high sedimentation-rate zones of the continental shelf, where the environment changes rapidly, the alteration processes are probably never completed (Giresse *et al.*, 1988). In favorable conditions, further transformation into glauconite may be possible.

ACKNOWLEDGMENTS

Our sincere thanks are due to D. Bish and S. Guggenheim for English language revision and invaluable critical comments and to D. Grabska for typing and editing this manuscript. The manuscript was reviewed by M. Amouric, who does not necessarily agree with all of the conclusions presented. We thank the referees, M. Amouric and A. Baronnet for comments that improved this paper.

REFERENCES

Amouric, M. and Parron, C. (1985) Structure and growth mechanism of glauconite as seen by high-resolution transmission electron microscopy. *Clays and Clay Minerals*, **33,** 473–482.

Amouric, M., Parron, C., Casalini, L., and Giresse, P. (1995) A (1:1) 7-Å Fe phase and its transformation in Recent sediments: An HRTEM and AEM study. *Clays and Clay Minerals*, **43,** 446–454.

Bailey, S.W. (1988) Odinite, a new dioctahedral-trioctahedral Fe^{3+}-rich 1:1 clay mineral. *Clay Minerals*, **23,** 237–247.

Elsass, F., Beaumont, A., Pernes, M., Jaunet, A.-M., and Tessier, D. (1998) Changes in layer organization of Na- and Ca-exchanged smectite materials during solvent exchanges for embedment in resin, *The Canadian Mineralogist*, **36,** 1475–1483.

Giresse, P. (1985) Le fer et les glauconies au large du fleuve Congo. *Sciences Geologiques, Bulletin*, Strasbourg, **38,** 293–322.

Giresse, P. and Odin, G.S. (1973) Nature minéralogique et origine des glauconies du plateau continental du Gabon et du Congo. *Sedimentology*, **20,** 457–488.

Giresse, P., Wiewióra, A., and Łącka, B. (1988) Mineral phases and processes within green peloids from two Recent deposits near the Congo River mouth. *Clay Minerals*, **23,** 447–458.

Giresse, P., Oualembo, P., Wiewióra, A., Łącka, B., and Zawidzki, P. (1992) Compositions polyphasées des grains verts du bassin du Congo; Comparaison de dépôts Récents, Holocènes (10^3–10^4 ans) et Miocènes (10^7 ans). *Archiwum Mineralogiczne*, **47,** 17–49.

Herbillon, A.J., Mestdagh, M.M., Vielvoye, L., and Derouane, E.G. (1976) Iron in kaolinite with special reference to kaolinite from tropical soils. *Clay Minerals*, **11,** 201–220.

Jepson, W.B. (1988) Structural iron in kaolinites and in associated ancillary minerals. In *Iron in Soil and Clay Minerals*, J.W. Stucki, B.A. Goodman, and U. Schwertmann, eds., NATO Advanced Study Institute Series, Series C: Mathematical and Physical Sciences, R. Reidel, Dordrecht, **217,** 467–536.

Malengreau, N., Muller, J.P., and Calas, G. (1994) Fe-speciation in kaolins: A diffuse reflectance study. *Clays and Clay Minerals*, **42,** 137–147.

Maley, J. (1996) The African rain forest—main characteristics of changes in vegetation and climate from the Upper Cretaceous to the Quaternary. *Proceedings of the Royal Society of Edinburgh*, **104B,** 31–73.

Mestdagh, M.M., Vielvoye, L., and Herbillon, A.J. (1980) Iron in kaolinite, II. The relationship between kaolinite crystallinity and iron content. *Clay Minerals*, **15,** 1–13.

Muller, J.P. and Calas, G. (1993) Genetic significance of paramagnetic centers in kaolinites. In *Kaolin Genesis and Utilization*, H.H. Murray, W.M. Bundy, and C.C. Harvey, eds., Clay Minerals Society of America, Boulder, Colorado, 261–289.

Nahon, D. (1981) Modes de répartition des métaux dans les solutions solides des altérations tropicales; applications aux concentrations supergènes ferrugineuses. In *Valorisation des Ressources du Sous-Sol*, D. Nahon, ed., Documents Bureau de Recherches Geologiques et Mineurs, Orléans, **47,** 254–264.

Odin, G.S., Bailey, S.W., Amouric, M., Fröhlich, F., and Waychunas, G.A. (1988) Mineralogy of the facies verdine. In *Green Marine Clays*, G.S. Odin, ed., Elsevier, Amsterdam, 159–206.

Oualembo-Mophawe, P.A. (1992) Les successions de grains verts argileux méso-cénozoïques du bassin marin congolais; paléoenvironnement, sédimentologie, minéralogie et géochimie. Ph.D. thesis, Univ. Perpignan, 335 pp.

Parron, C. (1989) Voies et mécanismes de cristallogénèse des minéraux argileux ferriferes en milieu marin. Le processus de glauconitisation: évolutions minérales, structurales et géodynamiques. Ph.D. thesis, Univ. Aix-Marseille, 411 pp.

Porrenga, D.H. (1967) Glauconite and chamosite as depth indicators in the marine environment. *Marine Geology*, **5,** 495–501.

Poumot, C. (1989) Palynological evidence for eustatic events in the tropical Neogene. *Centre Recherche Exploration Elf-Aquitaine Bulletin*, **13,** 437–453.

Sakharov, B.A., Besson, G., Drits, V.A., Kameneva, Y.U., Salyn, A.L., and Smoliar, B.B. (1990) X-ray study of the nature of stacking faults in the structure of glauconites. *Clay Minerals*, **25,** 419–435.

Séranne, M., Séguret, M., and Fauchier, M. (1992) Seismic super-units and post-rift evolution of the continental passive margin of southern Gabon. *Société Géologique de France Bulletin*, **163,** 135–146.

Siesser, W.G. (1978) Leg 40 results in relation to continental shelf and onshore geology. *Deep Sea Drilling Project, Internal Reports*, **40,** 965–979.

Stucki, J.W. (1988) Structural iron in smectites. In *Iron in Soils and Clay Minerals*, J.W. Stucki, B.A. Goodman, and U. Schwertmann, eds., NATO Advanced Study Institute Series, Series C: Mathematical and Physical Sciences, R. Reidel, Dordrecht, **217,** 625–675.

Środoń, J., Andreoli, C., Elsass, F., and Robert, M. (1990) Direct high-resolution transmission electron microscopic measurement of expandability of mixed-layer illite/smectite in bentonite rock. *Clays and Clay Minerals*, **38,** 373–379.

Von Gaertner, H.R. and Schellmann, W. (1965) Rezente Sedimente in Küstenbereich der Halbinsel Kaloun, Guinea. *Tschermaks Mineralogische und Petrographische Mitteilungen*, **10,** 349–367.

Warren, E.A. and Ransom, B. (1992) The influence of analytical error upon the interpretation of chemical variations in clay minerals. *Clay Minerals*, **27,** 193–209.

Wiewióra, A. (1990a) Crystallochemical classifications of phyllosilicates based on the unified system of projection of chemical composition: I. The mica group. *Clay Minerals*, **25,** 73–81.

Wiewióra, A. (1990b) Crystallochemical classifications of phyllosilicates based on the unified system of projection of chemical composition: III. The serpentine-kaolin group. *Clay Minerals*, **25,** 93–98.

Wiewióra, A., Łącka, B., and Giresse, P. (1996) Characterization and origin of 1:1 phyllosilicates within peloids of the Recent, Holocene and Miocene deposits of the Congo Basin. *Clays and Clay Minerals*, **44,** 587–598.

(Received 2 December 1997; accepted 5 April 1998; Ms. 97-110)